

Influence of track flexibility and spatial coherence of track irregularity on vehicle-slab track interaction

frequency-domain analysis

Xu, L.; Lu, T.

DOI

[10.1080/23248378.2020.1811170](https://doi.org/10.1080/23248378.2020.1811170)

Publication date

2020

Document Version

Final published version

Published in

International Journal of Rail Transportation

Citation (APA)

Xu, L., & Lu, T. (2020). Influence of track flexibility and spatial coherence of track irregularity on vehicle-slab track interaction: frequency-domain analysis. *International Journal of Rail Transportation*, 9 (2021)(4), 342-367. <https://doi.org/10.1080/23248378.2020.1811170>

Important note

To cite this publication, please use the final published version (if applicable). Please check the document version above.

Copyright

Other than for strictly personal use, it is not permitted to download, forward or distribute the text or part of it, without the consent of the author(s) and/or copyright holder(s), unless the work is under an open content license such as Creative Commons.

Takedown policy

Please contact us and provide details if you believe this document breaches copyrights. We will remove access to the work immediately and investigate your claim.



Influence of track flexibility and spatial coherence of track irregularity on vehicle-slab track interaction: frequency-domain analysis

Lei Xu & Tao Lu

To cite this article: Lei Xu & Tao Lu (2021) Influence of track flexibility and spatial coherence of track irregularity on vehicle-slab track interaction: frequency-domain analysis, International Journal of Rail Transportation, 9:4, 342-367, DOI: [10.1080/23248378.2020.1811170](https://doi.org/10.1080/23248378.2020.1811170)

To link to this article: <https://doi.org/10.1080/23248378.2020.1811170>



© 2020 The Author(s). Published by Informa UK Limited, trading as Taylor & Francis Group.



Published online: 08 Sep 2020.



Submit your article to this journal [↗](#)



Article views: 425



View related articles [↗](#)



View Crossmark data [↗](#)

Influence of track flexibility and spatial coherence of track irregularity on vehicle-slab track interaction: frequency-domain analysis

Lei Xu^a and Tao Lu ^b

^aSchool of Civil Engineering, Central South University, Changsha, China; ^bFaculty of Civil Engineering and Geosciences, Delft University of Technology, Delft, The Netherlands

ABSTRACT

A straightforward and practical method of frequency-domain analysis is developed for coupled vehicle-track system. The influence of the track flexibility and spatial coherence of irregularities on frequency response of vehicle-track systems are systematically studied accounting for train velocity and irregularity wavelength. Calculations show that the track flexibility cannot be ignored to obtain an accurate response of wheels whereas the resonance frequencies of car body motions remain unchanged. The inclusion of track flexibility enables consideration of wave reflections in rail sections between different wheels. The excitations at different wheels due to irregularity have phase lags determined by the train velocity and distances between wheels. This spatial coherence is important to the system response. The influence of contact spring on the system frequency response is examined. It is found that the system response converges at a certain value of the contact stiffness and the track stiffness governs the wheel-rail interaction after then.

ARTICLE HISTORY

Received 17 June 2020
Revised 3 August 2020
Accepted 13 August 2020



KEYWORDS

Vehicle-track interaction; frequency-domain response; track flexibility; receptance; track vertical irregularity; critical wavelength

1. Introduction

Vehicle-track interaction has been a long-standing topic in railway engineering since the last century. Due to the necessity of analysing nonlinearity of the wheel-rail contact, contact discontinuity such as hang sleeper, and some other nonlinear dynamic problems, time-domain analysis is widely applied to evaluate the system dynamic performance using the direct integration method. And also, remarkable developments have been made in the modelling and analysis of the vehicle-track interaction [1–3].

However, the deficiency of time-domain analysis is also obvious especially in figuring out the dynamic characteristics with high efficiency and precision due to its time-consuming nature. The frequency domain analysis is intrinsically more efficient. Frequency-domain analysis in structural dynamics can conveniently reveal the dynamic characteristics of a linear system with less computational efforts. The frequency components which may cause large system responses can be identified. For numerical modelling

CONTACT Tao Lu  T.Lu-2@tudelft.nl  Department of Engineering Structures, Faculty of Civil Engineering and Geosciences, Delft University of Technology, Stevinweg 1, Delft 2628 CN, The Netherlands

© 2020 The Author(s). Published by Informa UK Limited, trading as Taylor & Francis Group.
This is an Open Access article distributed under the terms of the Creative Commons Attribution-NonCommercial-NoDerivatives License (<http://creativecommons.org/licenses/by-nc-nd/4.0/>), which permits non-commercial re-use, distribution, and reproduction in any medium, provided the original work is properly cited, and is not altered, transformed, or built upon in any way.

of vehicle-track interaction, a comprehensive three-dimensional coupled vehicle-track system can consist of more than thousands degrees of freedom. One simulation in time-domain can cost relatively long time which is extremely not suitable for parametric study. It is therefore significantly important to seek a more direct and simple frequency analysis method for modelling vehicle-track interaction.

In railway engineering, receptance (displacement frequency response function) or mobility (velocity frequency response function) of railway tracks have been studied both theoretically and experimentally in a detailed manner for different track systems, e.g. conventional ballasted tracks [4–6] and slab tracks [7–10] without considering the vehicle effects. The track receptance is normally obtained considering one wheel-rail contact point except [11] in which the cross point receptances, namely the responses of the rail under different wheelsets excited by a harmonic point load under a specific wheelset were analysed. For the frequency-domain analysis, it is often the case that the track and the vehicle are considered separately. In a few references [12,13], frequency responses of railway system were analysed accounting for the vehicle effects by considering the unsprung wheel mass. It has been shown the coupling of the wheel is important to the frequency response of the track since the inclusion of wheel mass shifts the first resonance frequency to a lower value [12,13]. Similarly, when analysing dynamic responses of the vehicle excited by vertical track irregularities, the influence of track flexibility was shown to be important after 20 Hz in terms of contact forces [14] for conventional ballasted tracks. As stated in [15], ‘An accurate knowledge of wheel receptances is crucial to understand the wheel/rail interaction and its magnitude’. The coupling of track flexibility to the vehicle is therefore significant to obtain an accurate wheel receptances and receptances of other DOF of the vehicle. To summarize, when investigating the frequency-domain characteristics of a vehicle-track system, the two subsystems have to be accounted for simultaneously as a coupled system. This is rarely done for ballasted railway tracks, not to mention that the frequency response of a coupled slab track-vehicle system has not been addressed in the literature.

Besides, as one of the main sources of railway noise and vibration, track vertical irregularities, such as short-wavelength roughness on rail surfaces and long-wavelength unevenness from differential subgrade settlements, generate excitations whose frequency equals the passage velocity of the train divided by the wavelength of the irregularity. It is natural to expect that a combination of train velocity and wavelength of irregularity which leads to an excitation frequency of the same value as the resonant frequency components obtained from the frequency-domain analysis will cause a large response of the system. In the literature, the influence of track vertical irregularities on railway vehicle dynamics are widely discussed [16–18]. Critical wavelengths of track vertical irregularities which excite certain vehicle modes are investigated [16–19]. The investigations either do not take track flexibility into account [16,18] or the combined effect of wavelength of irregularities and train velocities are not considered [18]. In [17], both the ‘rigid track’ and flexible modelling for ballasted track scenarios are studied to examine the influence of the track flexibility on the vehicles. It is concluded that the track flexibility plays a minor role in vehicle dynamics in the frequency range 0–25 Hz. However, this frequency range does not cover the resonance peak of wheel vibration since the contact spring is relatively stiff and the wheel may vibrate at a frequency much higher than 25 Hz. Another important issue for irregularity excitations is that the spatial

coherence of multiple interaction points (multiple wheels). The excitations at different wheel-rail contact points have phase differences which are related to the distance between wheels and the train velocities. This coherence is studied in [18] in which the track is not modelled. However, without the track flexibility, the wave reflections between multiple wheels are not included although this wave phenomenon was proven to be important [19,20].

To make strides on the aforementioned studies, two contributions are made in the present study

- The frequency-domain characteristics of vehicle-slab track system with the subsystems fully coupled is thoroughly examined. The influence of the coupling is also addressed.
- The combined effects of train velocity and wavelength of irregularities in one goal in the framework of a fully coupled vehicle-slab track system is investigated.

Summarily, the organization of this work is as follow:

- In [Section 2](#), configuration of the vehicle-track interaction model and a brief introduction about the establishment method are elaborated.
- In [Section 3](#), the methods for achieving frequency- and time-domain solutions are presented.
- In [Sections 4 and 5](#), numerical studies are conducted systematically and conclusions are drawn.

2. Construction of the vehicle-track interaction model

Generally, the vehicle-track system consists of the vehicle subsystem and the track subsystem, being modelled as a multirigid-body system and flexible finite element system respectively. The two subsystems are coupled at the wheel-rail interfaces by satisfying force equilibrium and displacement compatibility between the wheel and the rail.

2.1. Configuration of the vehicle-track interaction system

The vehicle consists of a car body, two bogie frames and four wheelsets, and these rigid bodies are connected by the primary and the secondary suspensions characterized by spring-dashpot elements. The tracks consist of the rails at left- and right- side longitudinally modelled by Timoshenko beams, and track slabs modelled as thin-plate elements are distributed under the rail with specific spacing between adjacent track slabs. The rail-track slab interaction is characterized by discretely supported fasteners, and the subgrade is equivalently expressed as Winkler foundation.

To couple the vehicle and the tracks dynamically, it is of significantly importance to quantitatively formulate the wheel-rail interaction through forces, geometries and the matrices in highlight of the wheel/rail contact mechanism [1].

The configuration of the vehicle-track interaction model has been presented in [Figure 1](#), where the symbols y , z , ψ , β and θ denote the lateral, vertical, yaw, pitch and roll motion respectively; the subscripts 'c' and 'w' denote the car body and the wheelset respectively; the

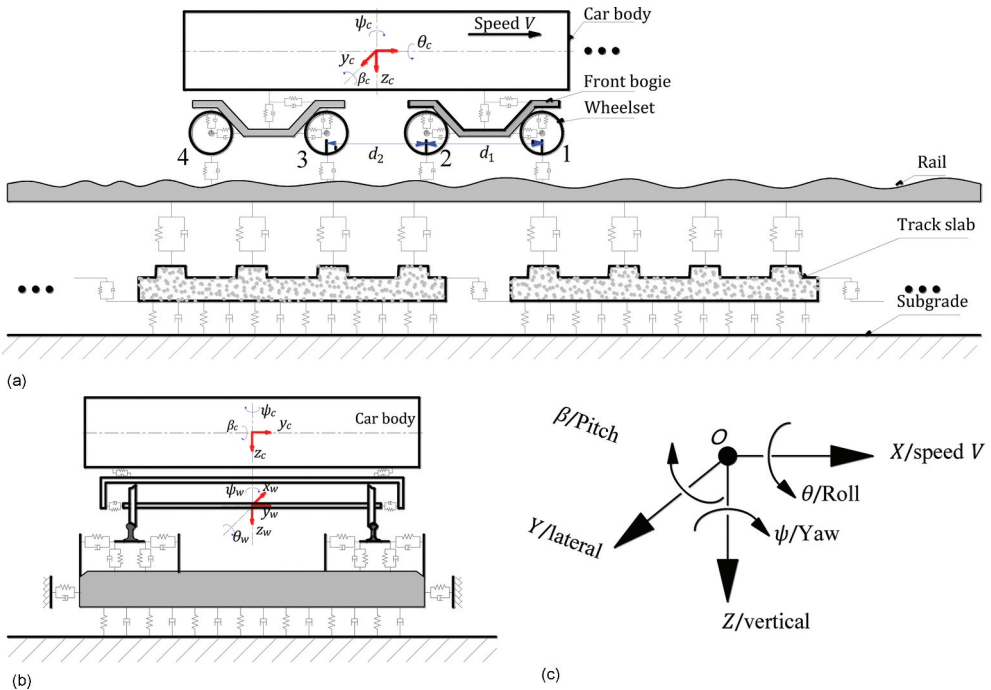


Figure 1. Vehicle-track interaction model (a) Side view; (b) End view; (c) Global coordinate system.

symbols ' k ' and ' c ' denote the stiffness and damping coefficient respectively; the subscripts 'p' and 's' denote the primary and secondary suspension system respectively and the subscripts ' x ', ' y ' and ' z ' denote the longitudinal-, lateral- and vertical- direction respectively.

2.2. Energy variation for deriving the wheel-rail interaction matrices

There are basically two methods to depict the wheel-rail interaction, as shown in Figure 2: the first method is explicitly calculating wheel-rail normal/creep forces by Hertz contact,

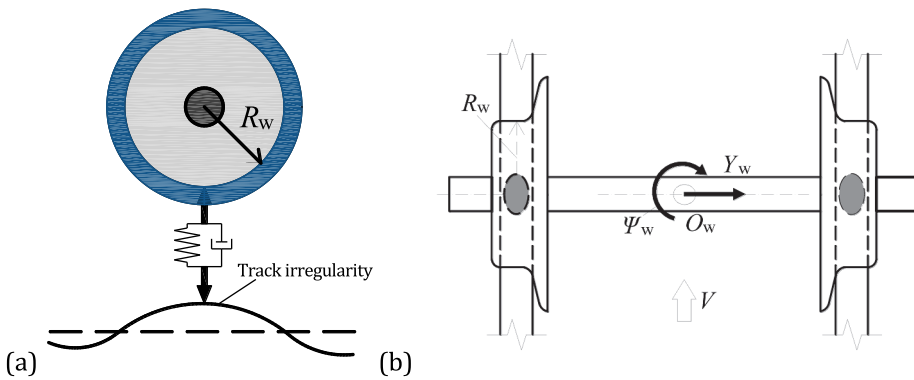


Figure 2. Wheel-rail interaction model: (a) Side view, (b) Top view.

Kalker’s linear creep theory with saturated-creep modification [1,4,5,11,15]; the second method is implicitly coupling the wheel and the rail by stiffness and damping matrices by energy variation principle [2].

Taking the second method as an example, the total elastic potential energy Π_d for the wheel-rail interaction can be assembled by

$$\Pi_d = \Pi_c + \Pi_k + \Pi_g + \Pi_{kg} \tag{1}$$

where Π_c is the negative value of the work done by the wheel-rail creep forces; Π_k is the elastic potential energy for the wheel-rail elastic compression; Π_g is the work done by the gravity and Π_{kg} is the work done by the gravitational restoring force/moment.

The negative value of the work done by the wheel-rail creep forces Π_c can be obtained as

$$\Pi_c = V_{c,x} + V_{c,y} + V_{c,z} + V_{c,\theta_z} \tag{2}$$

$$\begin{aligned} \text{with } V_{c,x} &= - \sum_i \sum_{j=l,r} F_{c,i,j}^x \Delta x_{c,i,j}^x, \quad V_{c,y} = - \sum_i \sum_{j=l,r} F_{c,i,j}^y \Delta x_{c,i,j}^y, \quad V_{c,z} = - \sum_i \sum_{j=l,r} F_{c,i,j}^z \Delta x_{c,i,j}^z, \\ V_{c,\theta_z} &= - \sum_i \sum_{j=l,r} F_{c,i,j}^{\theta_z} \Delta x_{c,i,j}^{\theta_z} \end{aligned}$$

where the symbol ‘ i ’ denotes the i th wheelset, and $j=l, r$ denote the left- and right- side of the wheelset respectively; F_c^x, F_c^y and F_c^z denote the longitudinal-, lateral- and vertical-creep force respectively and the $F_c^{\theta_z}$ denotes the spin moment; $\Delta x_c^x, \Delta x_c^y$ and Δx_c^z denote the wheel-rail relative longitudinal-, lateral- and vertical displacement and $\Delta x_c^{\theta_z}$ denotes the wheel-rail relative angle around Z -axis.

The elastic potential energy for the wheel-rail elastic compression Π_k can be obtained as

$$\Pi_k = \sum_i \sum_{j=l,r} \int_0^{\tilde{z}} k_{H,i,j}(\tilde{z}_{wr,i,j}) \tilde{z}_{wr,i,j} dz_{wr,i,j} \tag{3}$$

where k_H denotes the Hertz contact stiffness, and it is correlated to the wheel-rail elastic compression $\tilde{z}_{wr,i,j}$.

The work done by the gravity Π_g can be obtained as

$$\Pi_g = - \sum_i F_{g,i}^z z_{w,i} \tag{4}$$

where $F_{g,i}^z$ is the gravitational force borne by the i th wheelset; $z_{w,i}$ is the vertical displacement of the wheelset at the centroid.

The work done by the gravitational restoring forces Π_{kg} can be obtained as

$$\Pi_{kg} = \sum_i \left(F_{gy,i} \Delta z_{gy,i} + M_{gm,i} \psi_{w,i} \right) \tag{5}$$

where F_{gy} is the lateral gravitational restoring force and M_{gm} the restoring moment around Z -axis; $\Delta z_{gy,i}$ is the lateral relative displacement between the wheelset centroid and the centre of two side rails and $\psi_{w,i}$ is the yaw angle of the wheelset.

Following principle of total potential energy with stationary value, it can be got [21]

$$\delta_{\in} \Pi_d = 0 \quad (6)$$

where ‘ δ ’ denotes the variational symbol; the subscript ‘ \in ’ stresses that the variation is only conducted on the strain and displacement while the forces are kept constant in accordance with the virtual work principle.

Obviously, n dynamic equilibrium equations can be derived from Equation (1), and for every displacement parameter, the following equation should be satisfied, that is,

$$\delta C_i \frac{\partial \Pi_d}{\partial C_i} = 0 \quad (7)$$

With implementation of the ‘set-in-right-position’ rule in [22], the mathematical matrices formulations for wheel-rail interaction can be obtained.

Finally, the dynamic equations of motion for vehicle-track interaction can be assembled by matrix formulations

$$\begin{bmatrix} \mathbf{M}_{vv} & \mathbf{0} \\ \mathbf{0} & \mathbf{M}_{tt} \end{bmatrix} \begin{Bmatrix} \ddot{\mathbf{X}}_v \\ \ddot{\mathbf{X}}_t \end{Bmatrix} + \begin{bmatrix} \mathbf{C}_{vv} & \mathbf{C}_{vt} \\ \mathbf{C}_{tv} & \mathbf{C}_{tt} \end{bmatrix} \begin{Bmatrix} \dot{\mathbf{X}}_v \\ \dot{\mathbf{X}}_t \end{Bmatrix} + \begin{bmatrix} \mathbf{K}_{vv} & \mathbf{K}_{vt} \\ \mathbf{K}_{tv} & \mathbf{K}_{tt} \end{bmatrix} \begin{Bmatrix} \mathbf{X}_v \\ \mathbf{X}_t \end{Bmatrix} = \begin{Bmatrix} \mathbf{F}_v \\ \mathbf{F}_t \end{Bmatrix} \quad (8)$$

where \mathbf{M} , \mathbf{C} and \mathbf{K} denote the mass, damping and stiffness matrices respectively; the subscripts ‘ v ’ and ‘ t ’ denote the vehicle and the track structures; \mathbf{X} , $\dot{\mathbf{X}}$ and $\ddot{\mathbf{X}}$ denote the displacement, velocity and acceleration vector respectively, and \mathbf{F} denotes the loading vector.

The detail modelling method can further refer to Refs. [1,2], here not presented for brevity.

3. System response solution at frequency- and time- domain

3.1. Frequency-domain solution

3.1.1. Receptance

To obtain the dynamic characteristics of the vehicle-track coupled system in the frequency domain, the receptance (frequency response) of the system is investigated. After assembling the components of the mass, stiffness and damping matrices to obtain the global system matrices, the governing equations of the vehicle-track system can be written as follows in matrix form:

$$\mathbf{M}\ddot{\mathbf{x}} + \mathbf{K}\mathbf{x} + \mathbf{C}\dot{\mathbf{x}} = \mathbf{f} \quad (9)$$

where $\mathbf{M}, \mathbf{K}, \mathbf{C}$ are the $N \times N$ global mass, stiffness and damping matrices, respectively. In addition, $\mathbf{x}(t) = [x_1(t), \dots, x_N(t)]^T$ is the displacement vector and $\mathbf{f}(t) = [f_1(t), \dots, f_N(t)]^T$ is the force vector. It is defined that the receptance $\alpha_{i,j}$ is the frequency response of the i th degree of freedom under a unit harmonic load applied on the j th DOF (degree of freedom), namely $f_j(t) = 1 \cdot e^{i\Omega t}$. Because of the harmonic excitation, the force vector can be rewritten as $\mathbf{f}(t) = \mathbf{F} \cdot e^{i\Omega t}$ in which $\mathbf{F} = [F_1, \dots, F_N]^T$ is the force amplitude vector and the j th element $F_j = 1$ because of the unit amplitude of the harmonic excitation at the j th DOF. Under the harmonic excitation, the response can be written as follows:

$$\mathbf{x}(t) = \mathbf{X} \cdot e^{i\Omega t} = [X_1, \dots, X_N]^T \cdot e^{i\Omega t} \quad (10)$$

where \mathbf{X} is the amplitude vector of the displacement. After substitution of Equations (10) and (9), one obtains

$$[-\mathbf{M}\Omega^2 + \mathbf{K} + i\Omega\mathbf{C}]\mathbf{X} = \mathbf{F} \tag{11}$$

The receptance $\alpha_{i,j}$, namely the frequency response X_i of the i th degree of freedom ($1 \leq i \leq N$) can be obtained by solving Equation (9) after substitution Equation (10) to the latter. Note that the unit harmonic excitation can also be applied simultaneously on more than two degrees of freedom to represent excitations from a wheelset (two wheels) to both rails as is shown in [23]. Note that in such a case, the naming of receptance $\alpha_{i,j}$ is not applicable.

3.1.2. Response in the plane of velocity and wavelength of vertical irregularity

The harmonic excitation can come from different sources in practice. In this work, the rail vertical irregularity is considered. The so-called ‘moving irregularity’ approach is used to derive the system response with varying velocity of the train and wavelength of the irregularity. The vehicle-track coupled system is assumed to be excited by a vertical irregularity moving at the same speed v as the vehicle but in the opposite of the wheel rolling direction. The frequency Ω in Equation (10) becomes $\Omega = 2\pi v/\lambda = kv$ in which λ is the wavelength and k is the wavenumber of the irregularity, respectively. Thus, the time signature of the excitation can be expressed by $Ae^{i(2\pi v/\lambda)t}$ or Ae^{ikvt} and A is the amplitude of the irregularity.

The vehicle considered here consists two bogies with in total four wheelsets. The wheelsets are numbered from 1 to 4 in Figure 1(a). Assume the fourth wheelset is at $x = x_0$ where x_0 is the distance from the origin of coordinate, $d_1 = 2L_t$ is the distance between two wheelsets of one bogie and $d_2 = 2(L_c - L_t)$ is the distance between wheelset 2 and 3 as shown in Figure 1. The geometric parameters L_t and L_c are given in Table A1 in the Appendix. Therefore the excitation under the fourth wheelset is $Ae^{ik(vt+x_0)}$ and consequently, the excitation is $Ae^{ik(vt+x_0+d_1)}$ at the third wheelset, $Ae^{ik(vt+x_0+d_1+d_2)}$ at the second wheelset and $Ae^{ik(vt+x_0+2d_1+d_2)}$ at the first wheelset considering the phase shift. Now the vector \mathbf{f} in Equation (9) is the equivalent force vector due to the moving irregularity. The vertical degrees of freedom of wheels and the vertical degrees of freedom of the rail at the wheel-rail contact points will be directly excited by the vertical irregularity. Denoting the vertical degrees of the wheelsets as x_{w1z} to x_{w4z} , the vertical degrees of freedom right under those wheels are correspondingly designated as x_{w1L_rail} to x_{w4L_rail} for the left rail and x_{w1R_rail} to x_{w4R_rail} for the right rail.

Therefore, the equivalent force components applied on wheels are

$$\begin{cases} f_{w1z} = 2k_H \cdot Ae^{ik(x_0+2d_1+d_2)} \cdot e^{ikvt} \\ f_{w2z} = 2k_H \cdot Ae^{ik(x_0+d_1+d_2)} \cdot e^{ikvt} \\ f_{w3z} = 2k_H \cdot Ae^{ik(x_0+d_1)} \cdot e^{ikvt} \\ f_{w4z} = 2k_H \cdot Ae^{ik(x_0)} \cdot e^{ikvt} \end{cases} \tag{12}$$

The coefficient 2 comes from the fact that the wheelset is assumed to be a rigid body having only one freedom in vertical direction and it is supported by two Hertz contact springs on two rails. The equivalent force components applied to the track are

$$\begin{cases} f_{w1L_rail} = f_{w1R_rail} = -k_H \cdot A e^{ik(x_0+2d_1+d_2)} \cdot e^{ikvt} \\ f_{w2L_rail} = f_{w2R_rail} = -k_H \cdot A e^{ik(x_0+d_1+d_2)} \cdot e^{ikvt} \\ f_{w3L_rail} = f_{w3R_rail} = -k_H \cdot A e^{ik(x_0+d_1)} \cdot e^{ikvt} \\ f_{w4L_rail} = f_{w4R_rail} = -k_H \cdot A e^{ikx_0} \cdot e^{ikvt} \end{cases} \quad (13)$$

The other terms in \mathbf{f} are all zero.

Correspondingly, the response can be written as

$$\mathbf{x} = \mathbf{X} \cdot e^{ikvt} \cdot e^{ikx_0} = [X_1, \dots, X_N]^T \cdot e^{ikvt} \cdot e^{ikx_0} \quad (14)$$

where \mathbf{X} is the amplitude vector of the displacement. Upon substitution of the force to Equation (9), one obtains:

$$[-\mathbf{M}(kv)^2 + \mathbf{K} + i(kv)\mathbf{C}]\mathbf{X} = \mathbf{F} \quad (15)$$

where $\mathbf{F} = [F_1, \dots, F_N]^T$ in which

$$\begin{cases} F_{w1z} = 2k_H \cdot A e^{ik(2d_1+d_2)} \\ F_{w2z} = 2k_H \cdot A e^{ik(d_1+d_2)} \\ F_{w3z} = 2k_H \cdot A e^{ikd_1} \\ F_{w4z} = 2k_H \cdot A \end{cases} \quad \text{and} \quad \begin{cases} F_{w1L_rail} = F_{w1R_rail} = -k_H \cdot A \exp(ik(2d_1 + d_2)) \\ F_{w2L_rail} = F_{w2R_rail} = -k_H \cdot A \exp(ik(d_1 + d_2)) \\ F_{w3L_rail} = F_{w3R_rail} = -k_H \cdot A \exp(ikd_1) \\ F_{w4L_rail} = F_{w4R_rail} = -k_H \cdot A \end{cases} \quad (16)$$

The other entries in \mathbf{F} are all zero. The response X_i of an arbitrary i th degree of freedom ($1 \leq i \leq N$) can be obtained by solving Equation (16). The value of x_0 is chosen arbitrarily since the term e^{ikx_0} is cancelled when solving Equation (16).

Generally frequency domain solution is developed to solve linear problems and it is rather convenient to reveal the system frequency characteristics.

3.2. Time-domain solution

To obtain time-domain solution of vehicle-track systems by excitations, such as track irregularities, with random combinations of wavelengths and phase, sometimes, with parametric nonlinearity and discontinuity, the time integration scheme such as Newmark- β and Wilson- θ can be applied to derive the system response at time domain.

Set Newmark- β as an example, the following steps can be followed to obtain system responses:

Forming the vehicle-track coupling matrices: mass matrix \mathbf{M}_{vt} , damping matrix \mathbf{C}_{vt} , stiffness

matrix \mathbf{K}_{vt} ,

Computing the equivalent stiffness matrix: $\bar{\mathbf{K}}_{vt} = \mathbf{K}_{vt} + \frac{1}{\beta\Delta t^2} \mathbf{M}_{vt} + \frac{\gamma}{\beta\Delta t} \mathbf{C}_{vt}$,

Deriving the equivalent loading vector:

$$\begin{aligned} \bar{\mathbf{F}}_{vt} = & \mathbf{F}_{vt} + \mathbf{M}_{vt} \left[\frac{1}{\beta\Delta t^2} \mathbf{X}_t + \frac{1}{\beta\Delta t} \dot{\mathbf{X}}_t + \left(\frac{1}{2\beta} - 1 \right) \ddot{\mathbf{X}}_t \right] \\ & + \mathbf{C}_{vt} \left[\frac{\gamma}{\beta\Delta t} \mathbf{X}_t + \left(\frac{\gamma}{\beta} - 1 \right) \dot{\mathbf{X}}_t + \frac{\Delta t}{2} \left(\frac{\gamma}{\beta} - 2 \right) \ddot{\mathbf{X}}_t \right], \end{aligned}$$

with $\mathbf{F}_{vt} = -\tilde{\mathbf{M}}_{vt}\ddot{\mathbf{X}}_t^I - \tilde{\mathbf{C}}_{vt}\dot{\mathbf{X}}_t^I - \tilde{\mathbf{K}}_{vt}\mathbf{X}_t^I$, where $\tilde{\mathbf{M}}_{vt}$, $\tilde{\mathbf{C}}_{vt}$ and $\tilde{\mathbf{K}}_{vt}$ denote the original mass, damping and stiffness matrix respectively;

Obtain the displacement vector at time $t + \Delta t$:

$$\mathbf{X}_{t+\Delta t} = \bar{\mathbf{K}}_{vt}^{-1}\bar{\mathbf{F}}_{vt},$$

Obtain the acceleration and velocity vector at time $t + \Delta t$:

$$\ddot{\mathbf{X}}_{t+\Delta t} = \frac{1}{\beta\Delta t^2}(\mathbf{X}_{t+\Delta t} - \mathbf{X}_t) - \frac{1}{\beta\Delta t}\dot{\mathbf{X}}_t - \left(\frac{1}{2\beta} - 1\right)\ddot{\mathbf{X}}_t,$$

$$\dot{\mathbf{X}}_{t+\Delta t} = \dot{\mathbf{X}}_t + \Delta t(1 - \gamma)\ddot{\mathbf{X}}_t + \Delta t\gamma\ddot{\mathbf{X}}_{t+\Delta t},$$

After the acquisition of the time-domain responses of indices, amplitude-frequency spectra based on Fourier transformation can be also assessed.

Generally, time-domain solution is developed to solve nonlinear and time-dependent problems.

4. Numerical studies

In the numerical studies, comparisons between the time- and frequency- domain responses are firstly presented to show the effectiveness of the solutions, and then systematical studies are conducted to reveal the track flexibility and spatial coherence of track irregularities on system frequency response, and parametric studies are also presented to illustrate the wheel/rail contact stiffness on frequency response variations. The computational domain is chosen as such the influences of the vehicle are fully damped at the boundaries.

The parameters used in the examples are listed in [Tables A1](#) and [A2](#) in the Appendix.

4.1. Comparisons between time- and frequency- domain solutions

In vehicle-track interaction, power spectral density of track irregularities, denoted as \mathbf{S}_{xx} , is generally applied as system excitations. Following the equivalent transformation between power spectral density and signal amplitude [24], the amplitude of A transformed as the wheel/rail interfacial excitation in [Equations](#), (12), (13) and (16) can be obtained as

$$A = \sqrt{S_{xx}(\tilde{\omega})} \quad (17)$$

where $\tilde{\omega}$ is the circular frequency.

The vehicle speed is setting to be 250 km/h. In the frequency domain analysis, the Hertz contact stiffness is linear. According to K.L. Johnson's research [25], the contact stiffness can be estimated by formula

$$k_H = \frac{3}{2}F_s^{1/3} \left[\frac{2}{3} \frac{E}{1 - \nu^2} (r_w r_r)^{1/4} \right]^{2/3} \quad (18)$$

where F_s is the wheel static load; E is the elastic modulus of the wheel and the rail and ν is the Poisson ratio; r_w and r_r are respectively the contact curve radius of the wheel and the

rail, For the real case considered in this work, k_H can be obtained as $3.1 \times 10^7 F_s^{1/3}$. If $F_s=79$ kN, $k_H=1.3$ GN/m, however, if considering the dynamic effects of rail irregularities and assuming that the wheel-rail contact deformation is less than 2 mm, k_H can be estimated as 4.6 GN/m approximately. Hence this study chooses two stiffness of soft 0.1 GN/m and hard 8 GN/m except the static one 1GN/m, to achieve more clear comparisons.

Through comparisons on power spectral density function, $S_{yy}(\omega) = Y(\omega)^* Y(\omega)^T$, $Y(\omega)$ is the amplitude spectrum, [Figure 3](#) plots the comparisons on dynamic indices of car body acceleration and wheel-rail force between the time domain solution and the frequency domain solution. It can be observed from [Figure 3](#) that similar results have been obtained for these two solutions especially when the Hertz contact stiffness reaches 1 GN/m and 8 GN/m. However, the differences of results between the time domain solution and frequency domain solution are large if the Hertz contact stiffness is too soft to be 0.1 GN/m, which is also indicating that the wheel-rail contact stiffness exerts significant influence on system frequency response performance.

4.2. Frequency domain analysis of the vehicle

The frequency response in terms of displacement is investigated in this section following the procedure described in [Section 3.1](#). In studies of vehicle-track interaction, acceleration is an important indicator. The acceleration frequency response (accelerance) can be readily obtained as the production of the displacement frequency response (receptance) and $-\Omega^2$. Although the resonant frequencies of the receptance and the accelerance are different. The difference is marginal provided the damping values are small, which is normally the case.

4.2.1. Frequency response: comparison between rigid and flexible track cases

The frequency response of the vehicle is calculated for two cases: (a) the track flexibility is not included, namely the track is considered as rigid and the contact spring is kept at the wheel track interface; (b) the vehicle is coupled with the track and therefore the flexibility of the track is included. For the two cases, a unit point harmonic load $1 \cdot \exp(i\Omega t)$ is applied on the degree of the vertical motion of the fourth wheelset. The positions of wheelsets are not important for rigid track case since no waves are generated in the rail reflecting between wheelsets and bogies. For the vehicle-track coupled case, the location of excitations matters because of: (1) periodic change of track properties due to discretely positioned rail fasteners; (2) Waves generation in rails and reflecting of these waves between wheelsets and bogies. The main features of vehicle response will keep the same regardless of the excitation position. The fourth wheelset is chosen as a reference. Without loss of generality, the fourth wheelset is assumed to be on the railseat, namely above a rail fastener. The parameters used are listed in the Appendix. [Figure 4](#) shows the frequency response of the car body. The unit harmonic excitation is placed on the degree of vertical motion of the fourth wheelset. One can see that car body bouncing motion resonates at 0.7 Hz whereas resonance of the pitch motion of car body occurs at 0.93 Hz from [Figure 4\(a\)](#) for the rigid track case. The peak at 93.5 Hz in [Figure 4\(a\)](#) is related to the vibration of unsprung mass on the Hertz contact spring. This is confirmed by

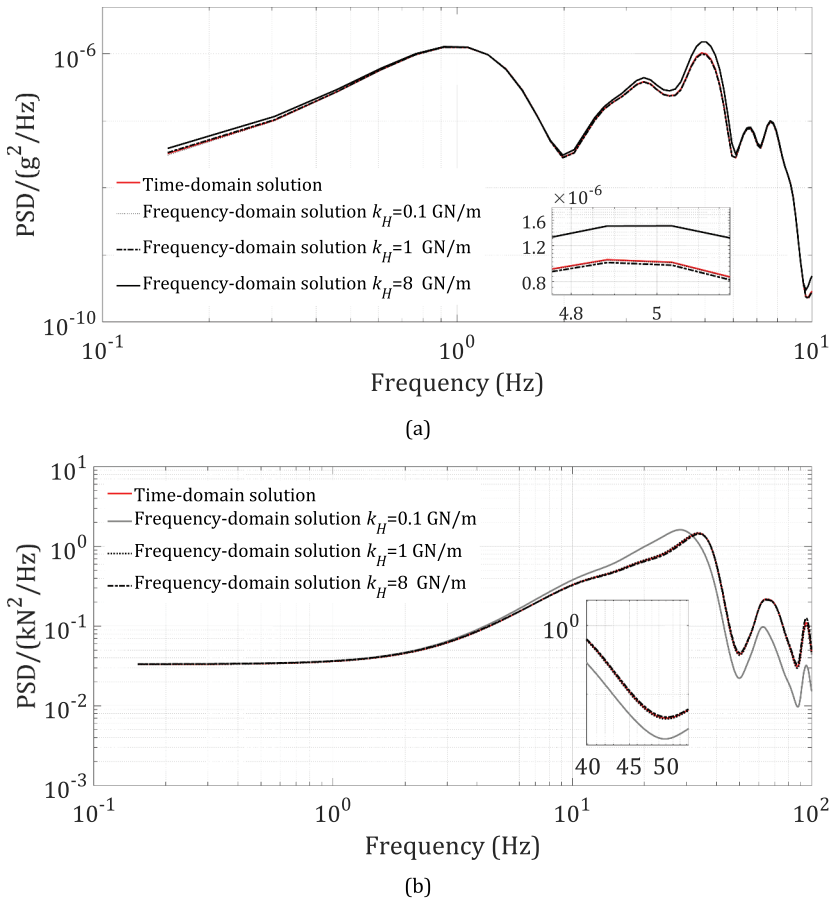


Figure 3. Comparisons between time-domain and frequency-domain solutions: (a) Car body vertical acceleration, (b) Wheel-rail vertical force.

examining the driving point displacement FRF, namely the displacement at wheelset 4 caused a vertical harmonic excitation at wheelset 4 by calculating:

$$\frac{\sqrt{k_H/m_w}}{2\pi} = \frac{\sqrt{3 \cdot 10^8/(1680/2)}}{2\pi} = 95.1 \text{ Hz} \tag{19}$$

in which m_w is half of the mass of one wheelset M_w as listed in Table A1 in the Appendix. When the track flexibility is considered as shown in Figure 4(b), the car body motions are not influenced since the resonance frequencies of the bouncing and pitch motions are not changed. However, the driving point displacement FRFs at wheelset 4 are affected since the contact force changes when the displacement of the track is included. Now the wheel vibrates on the combined stiffness of the contact spring and the track, results in a downshift of the resonance peak to about $f_w = 32.7\text{Hz}$.

Figures 5 and 6 demonstrate frequency responses of bogies. The frequency response is plotted till 200 Hz only since the vibrations of vehicle are mainly in the low frequency range. The first and main resonance peak of the vertical motion of bogies is at $f_{cv} = 0.74\text{Hz}$. This frequency corresponds mainly to bogie bouncing

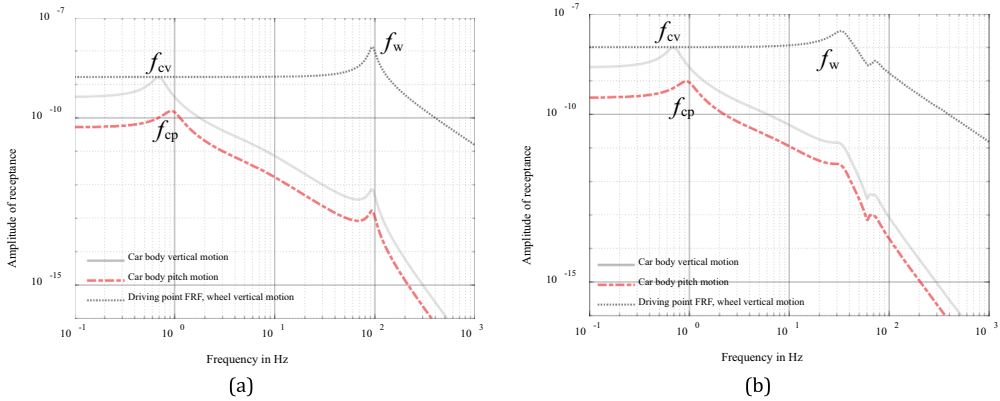


Figure 4. Car body response: (a) Rigid track, (b) Track flexibility included.

motion. The first peak of pitch motion of bogies is $f_{cp} = 0.93\text{Hz}$ at which the pitch motion of car body dominates as shown in Figure 4. The second peak at 6.2 Hz is associated with dominating bogie pitch. One can see that the amplitudes of motions of the front bogie are smaller than those of the rear bogies, and peaks are more obvious for the front bogie as well. This is due to the fact that the excitation is placed on the fourth wheel which is attached to the rear bogie. The motion of the rear bogie is mainly governed by the excitation directly whereas the front bogie is also influenced by waves propagating from the excited wheel to wheels of the front bogie. At higher frequencies, taking into account the track flexibility results in multiple peaks, e.g. in Figure 5(b) due to wave reflections in rail sections between bogies and wheelsets which will form standing waves at certain frequencies in those rail sections. However, when the track flexibility is not included, such wave reflections are not possible because no elastic waves exist in rigid track.

Another observation from Figures 4–6 is that the responses of the vehicle with track flexibility included are lower than those with rigid track assumption, as expected.

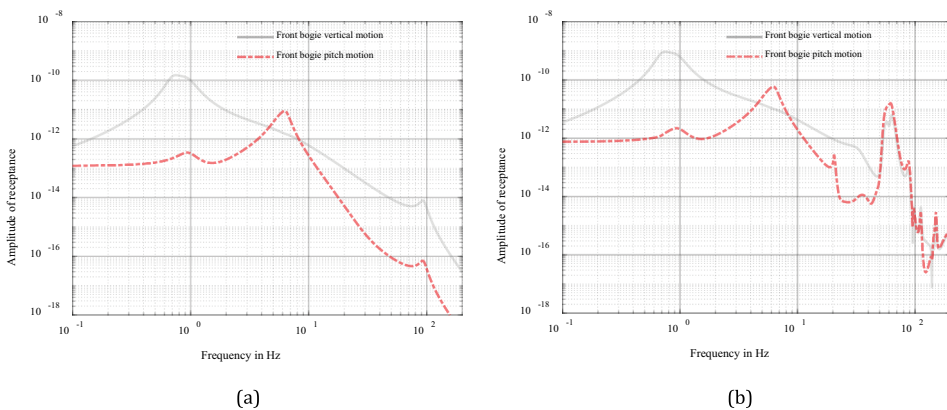


Figure 5. Front bogie response: (a) Rigid track, (b) Track flexibility included.

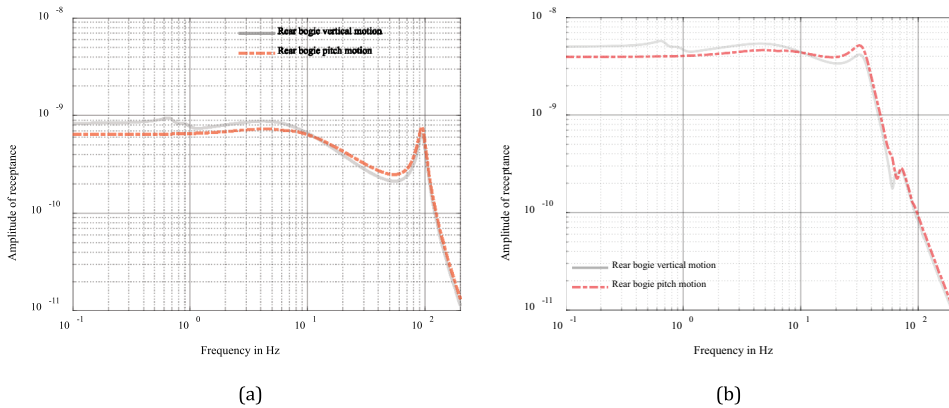


Figure 6. Rear bogie response: (a) Rigid track, (b) Track flexibility included.

4.2.2. Response in wavelength and velocity plane

The responses in the wavelength and velocity plane are calculated in this section from Equation (15). This analysis aims to identify combinations of velocity and wavelength which lead to resonant responses of the vehicle. The range of wavelength of irregularities considered is 0.1 ~ 20 m with exception when investigating car body pitch motion. Typical wavelengths of track irregularities on high-speed railway lines in China are within this range [26]. The velocity is calculated from 10 km/h till 400 km/h.

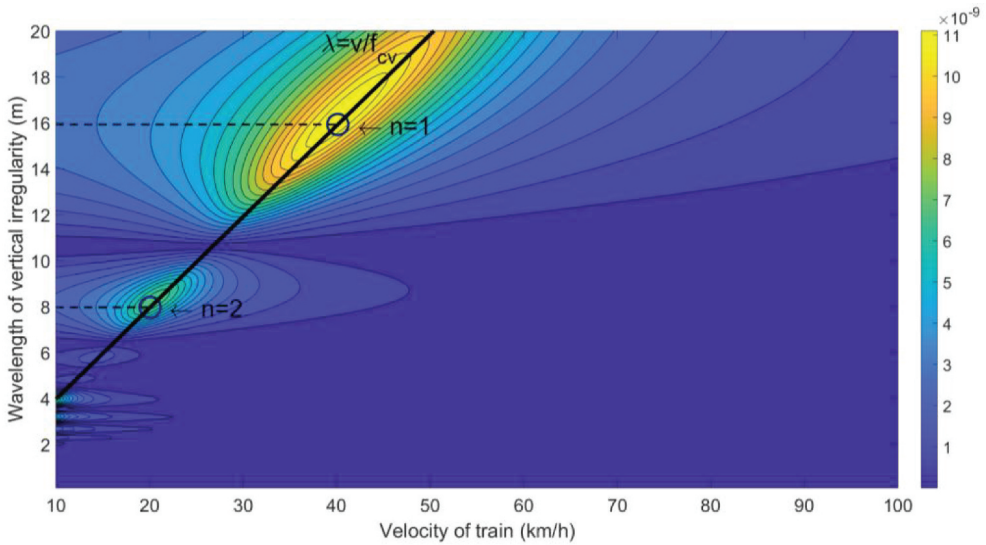
In Figure 7(a), the response of car body vertical motion is shown in the contour plot. For a better visibility, the velocity is plotted till 140 km/h since generally the response is large at long wavelength and low train velocity [27]. The reason is that this combination leads to small excitation frequency in the range of natural frequency of the car body. To excite the vertical motion, it is expected that resonance occurs when $f_{ex} = v/\lambda = f_{cv}$ in which $f_{cv} = 0.74\text{Hz}$ is the resonant frequency of car body vertical motion as shown in Figure 4. This is confirmed in Figure 7(b). Two wavelengths are chosen to plot the response versus the velocity (this plot is actually a slice of the contour plot). A second x-axis which represents excitation frequency calculated by $f_{ex} = v/\lambda$ is added. It is clearly shown that resonance occurs at train velocities which give rise to excitations of frequency $f_{ex} = f_{cv}$. In Figure 7(a), the resonance condition

$$\lambda = v/f_{cv} \tag{20}$$

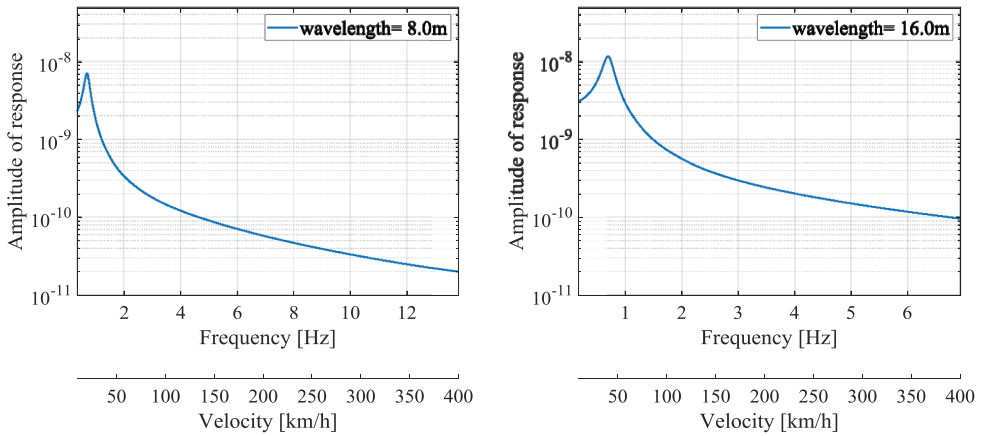
for the vertical car body motion is plotted. Since the vertical motion of the car body is a symmetric mode, the maximum amplitude of this motion is excited by the irregularity when the two bogies move in-phase. To satisfy this condition, the wavelength of the irregularity should satisfy [3]

$$\lambda = (d_1 + d_2)/n, \quad n = (1, 2, 3\dots). \tag{21}$$

Therefore, maximum responses occur at discrete locations defined by Equation (21) on the line of Equation (20). The velocities at these discrete points in Figure 4(a) are called critical velocities of a certain vibration mode (here dominantly the vertical car body motion). Theoretically, there are an infinite number of combinations of wavelength and velocity defined by Equations (20–21) for the vertical motion as can be seen in Figure 7(a)



(a)



(b)

Figure 7. Carbody vertical motion, normalized with respect to $k_H \cdot A$: (a) Response of car body vertical motion in λ and v plane, (b) Frequency response of car body vertical motion for certain wavelengths of irregularities.

in the lower wavelength and velocity regions, as well as the pitch motion which will be shown later. However, only the highest critical speeds are suitable for inserting enough energy to excite the car body motions since the amplitudes of the harmonic components and the associated energy introduced in the system by the track irregularities reduce with decreasing wavelength as pointed out in [17]. $n = 1$ and 2 are plotted for Equation (11) in Figure 7(a). It confirms this statement as the highest critical velocity $v = 40\text{km/h}$ at $n = 1$ gives the largest magnitude of response.

Figure 8 shows the response of the car body pitch motion. When the combination of irregularity wavelength and train velocity leads to an excitation frequency $f_{\text{ex}} = v/\lambda$ coinciding with the resonant frequency of car body pitch motion $f_{\text{cp}} = 0.93\text{Hz}$ as shown in Figure 7, peak motion occurs. Two slices of the contour plot are shown in Figure 8(b) in which resonance can be observed at 0.93 Hz.

In addition, the pitch motion is an antisymmetric motion. Resonance occurs when the rear and front bogies are excited out-of-phase by the irregularity. Therefore, Equation (21) becomes [17]

$$\lambda = 2(d_1 + d_2)/(2n - 1), \quad n = (1, 2, 3, \dots). \quad (22)$$

Therefore, now Equations (20) and (22) govern the critical velocities. In Figure 8, $n=1-3$ is plotted for Equation (22). The highest critical velocity for the car body pitch motion is seen at $v = 106.6\text{km/h}$ for a wavelength of 31.8 m.

From Figures 9–12 the vertical responses of all the four wheelsets are plotted. Again a contour plot in $\lambda - v$ plane and a slice of the contour plot at a specific wavelength is presented. We denote f_w as the resonant frequency of vertical motion of the wheelsets as shown in Figure 7. One can conclude that for all the wheels resonance occur at the same frequency $f_{\text{ex}} = v/\lambda = f_w = 32.7\text{Hz}$ which is the bright band in the contour plot. At this frequency the wheel vibrates on the combined stiffness of the track and the contact spring as shown in Figure 4(b). The different locations of the wheels do not influence the resonant frequency. Since the resonance frequency is relatively high, long-wavelength irregularities will not lead to the resonance frequency in the operational velocity range of current high-speed trains, the wavelength is plotted till 5 m in Figures 9–12 for better visibility. In all the Figures 9–12, a slice is taken from the contour plot for $\lambda = 2.0\text{m}$. The slices indicate clearly the main resonance of the wheelsets' vertical motion occurs at f_w .

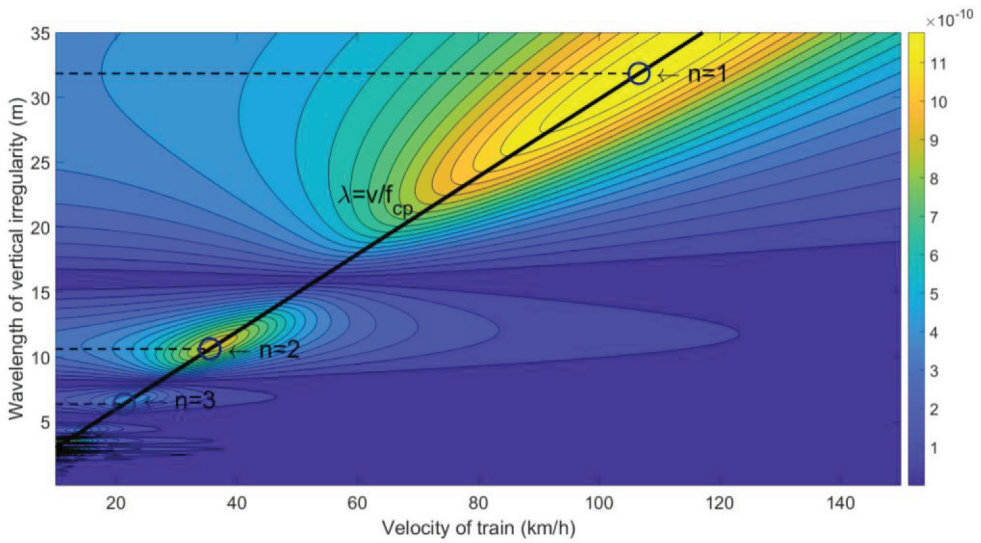
Because the motions of bogies are largely dependent on the distances between bogies and wheelsets, no universe rules apply, and here the responses of the bogies are not present.

To conclude, the spatial correlation of excitations at different wheels must be considered to predict critical wavelength and vehicle speed combinations which excite certain vehicle modes, e.g. carbody vertical and pitch motions. Similar conclusions can also be found in [17,18].

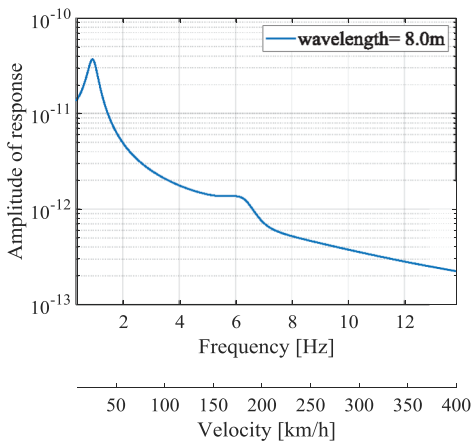
4.3. Frequency domain analysis of the rail

4.3.1. Frequency response: comparison between coupled- and uncoupled vehicle conditions

The frequency response of the rail is calculated for two cases: (a) the vehicle is not included; (b) the vehicle is coupled with the track and therefore the vehicle-track interaction is considered. For the two cases, two unit point harmonic loads $1 \cdot \exp(i\Omega t)$ are applied symmetrically on the degrees of the vertical motion of the two rails on the railseat and the mid-span of two adjacent railseats. When vehicle is coupled, the fourth wheelset is placed on the same position to the applied force.



(a)



(b)

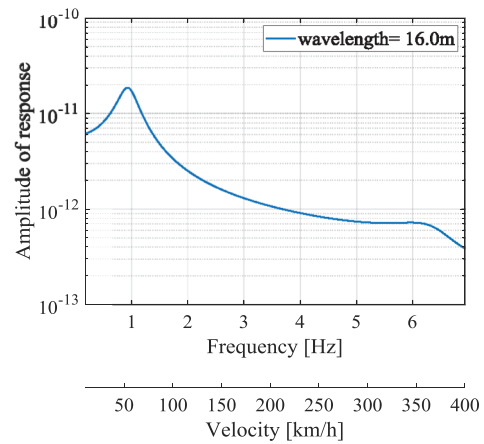


Figure 8. Car body pitch motion, normalized with respect to $k_H \cdot A$: (a) Response of car body pitch motion in λ and v plane, (b) Frequency response of the car body pitch motion for certain wavelengths of irregularities.

As shown in Figure 13, when vehicle is included, the first resonance peak f_r of the track receptance is shifted from 52 Hz to a lower value of 33 Hz. This is expected because consideration of the vehicle leads to an increasing of overall mass to the track and thus the resonance frequency decreases. The pinned-pinned frequency at 1062 Hz of the rail is not influenced by accounting for the vehicle or not. However, when the vehicle is considered, the response of the rail at mid-span becomes lower than the case without vehicle at the pinned-pinned frequency. The antiresonance frequency a bit less than 100 Hz in Figure 13(b) corresponds to wheel resonance which is given by Equation (19).

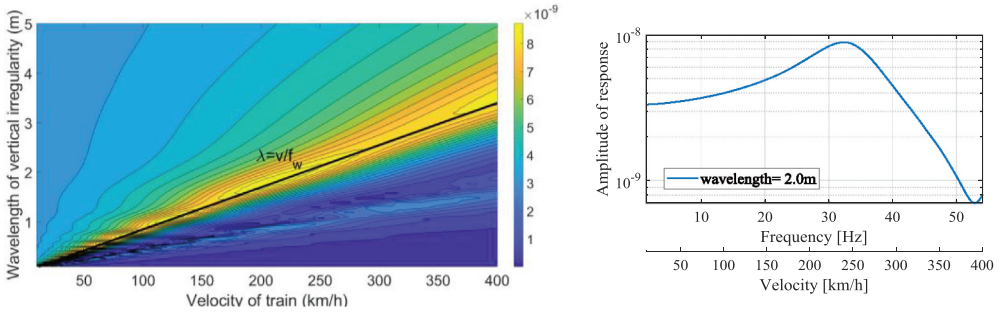


Figure 9. First wheelset vertical motion, normalized with respect to $k_H \cdot A$.

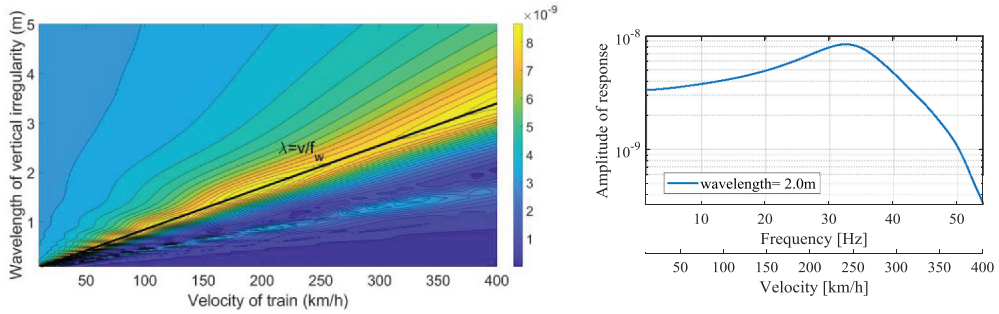


Figure 10. Second wheelset vertical motion, normalized with respect to $k_H \cdot A$.

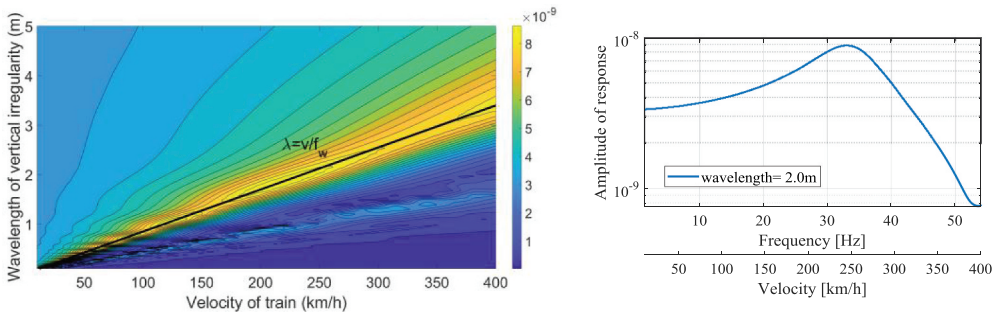


Figure 11. Third wheelset vertical motion, normalized with respect to $k_H \cdot A$.

4.3.2. Response in the velocity and wavelength of the irregularities

In Figures 14–17 the vertical responses of the rail at four positions directly under the four wheelset are presented. A contour plot in $\lambda - v$ plane and a slice of the contour plot at a specific wavelength is plotted. The maximum rail displacement occurs at $f_{ex} = v/\lambda \approx f_T$ (the bright area in the contour plots) which corresponds to the peak of the track receptance as shown in Figure 13. It can be concluded that the resonance frequency is not influenced by the locations of the track. The wavelength is plotted till 5 m in Figures 14–17 for better visibility. For longer wavelengths, the vertical response of the rail is relatively small.

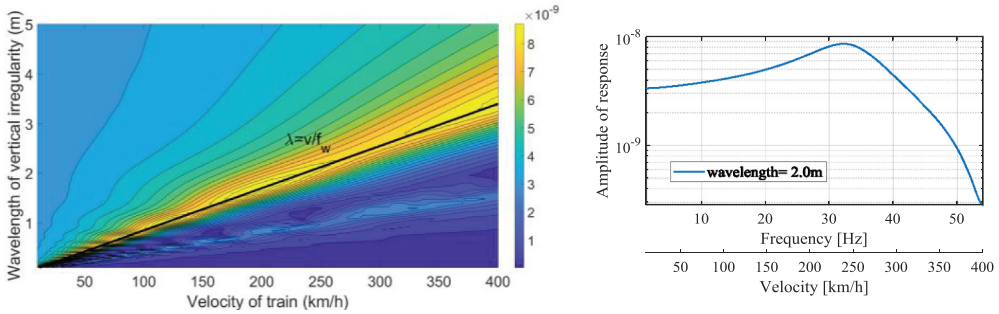


Figure 12. Fourth wheelset vertical motion, normalized with respect to $k_H \cdot A$.

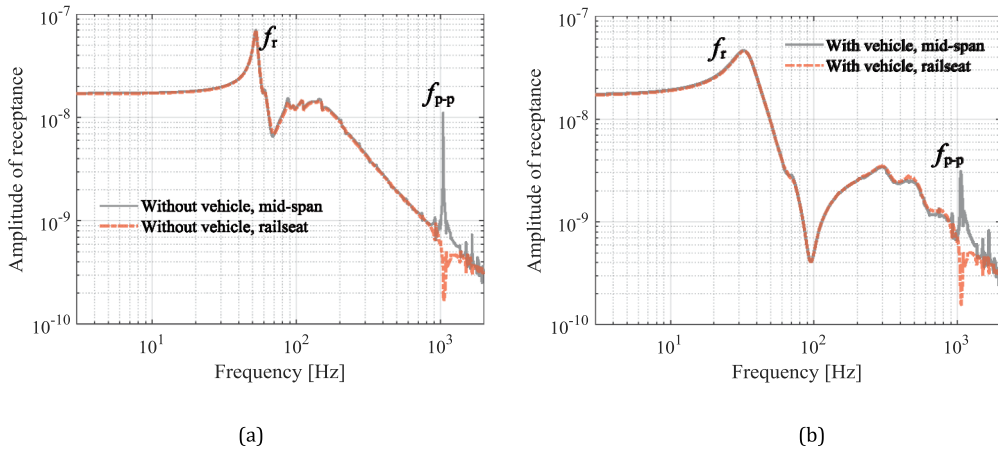


Figure 13. Driving point receptance of rail: (a) Driving point track receptance, without vehicle, the first peak is at 52 Hz, (b) Driving point track receptance, with vehicle, first peak at 33 Hz.

4.4. Influence of the stiffness of the contact spring

From Figures 18–21, the influence of the stiffness of the contact spring is analysed. The responses are normalized with respect to the amplitude of the irregularity. In other words, the comparisons are made considering the same irregularity thus the influences of the contact spring are solely extracted. In general, it can be concluded that higher stiffness of the contact spring leads to a higher response level because of larger contact force. The stiffness change does not influence the resonance frequencies of the car body bouncing, car body pitch, bogie bouncing and bogie pitch motions. In contrast, greater stiffness of the contact spring results in an increase of the resonance frequency of the wheel vertical motion as shown in Figure 21. As can be seen that there is almost no difference in the responses between $k_H = 1.0\text{GN/m}$ and $k_H = 8.0\text{GN/m}$, the influence of contact spring on resonance frequencies of the vehicle becomes marginal when k_H keeps increasing. This observation can be explained as the following: when k_H increases, the wheel-track contact becomes more and more rigid, then the track stiffness dominates the response.

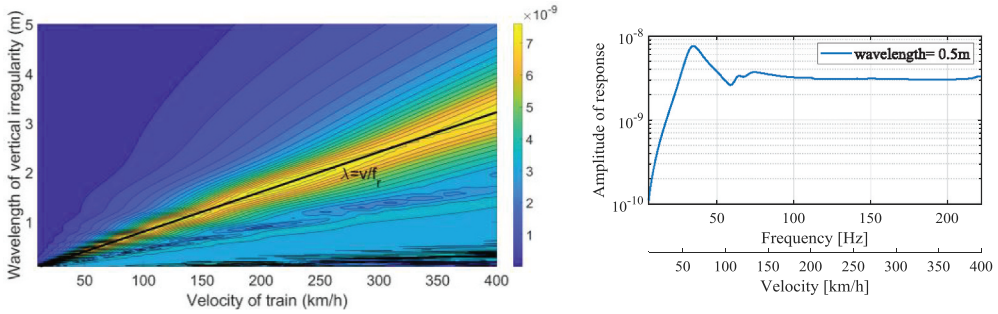


Figure 14. Vertical motion of rail under first wheelset, normalized with respect to $k_H \cdot A$.

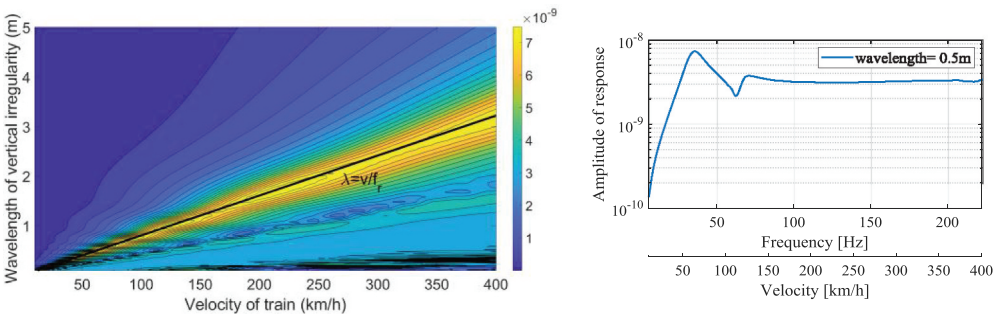


Figure 15. Vertical motion of rail under second wheelset, normalized with respect to $k_H \cdot A$.

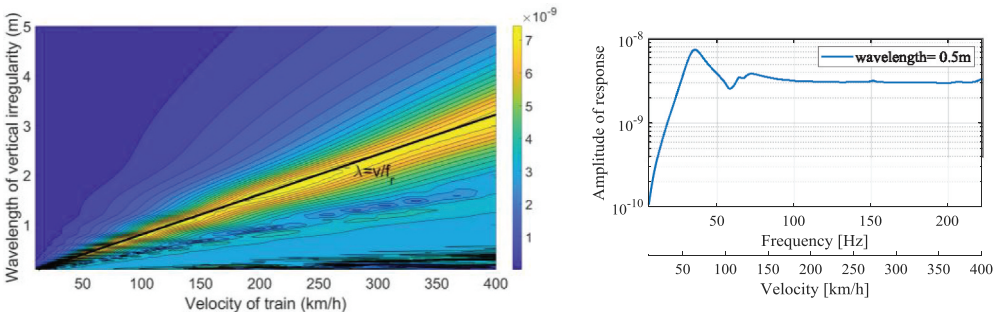


Figure 16. Vertical motion of rail under third wheelset, normalized with respect to $k_H \cdot A$.

In Figure 22, the receptance of the rail is calculated for three values of contact stiffness. The contact spring play a minor role on the wheel-rail interaction especially in low frequency regions in which the vehicle responses and first resonance peak of the rail are most relevant. However, the antiresonance frequency of the rail is largely influenced by the contact stiffness since this frequency corresponds to resonance of wheel motion as predicted by Equation 19. To visualize the location of this frequency, the receptances of contact spring and unsprung mass are plotted as well. Antiresonance occurs at the intersection of contact spring receptance and unsprung mass receptance as shown in Figure 22.

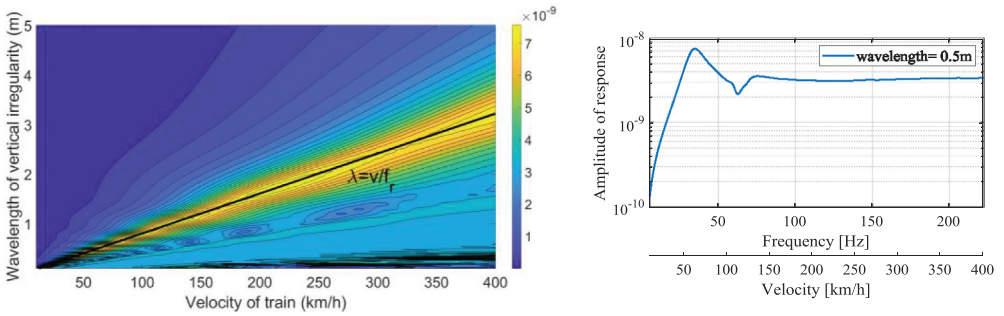


Figure 17. Vertical motion of rail under fourth wheelset, normalized with respect to $k_H \cdot A$.

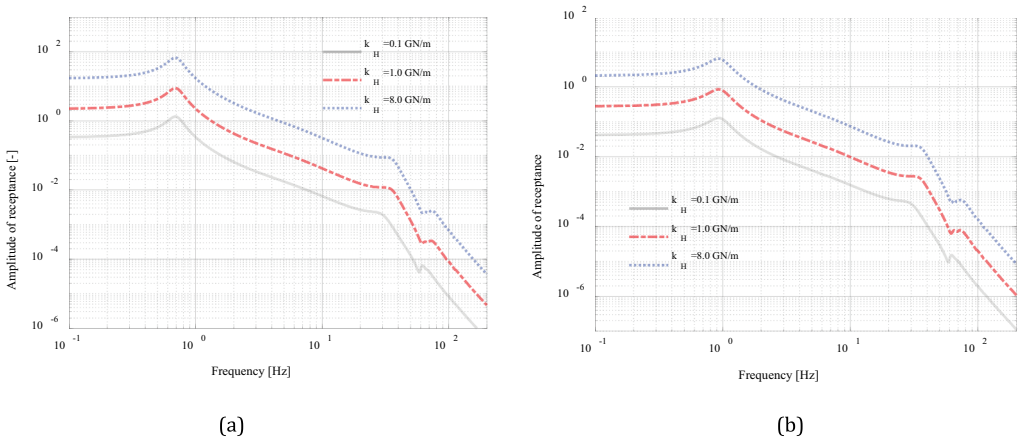


Figure 18. Car body response, normalized with respect to A : (a) Vertical motion, (b) Pitch motion.

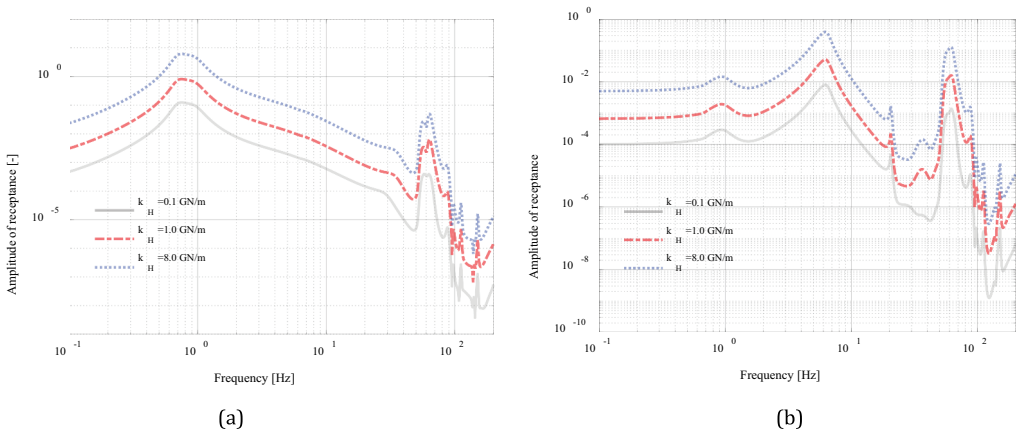


Figure 19. Front bogie response, normalized with respect to A : (a) Vertical motion, (b) Pitch motion.

Larger stiffness of contact spring leads to an intersection at higher frequency and the amplitude of the response decreases accordingly. From Figure 22 it can be

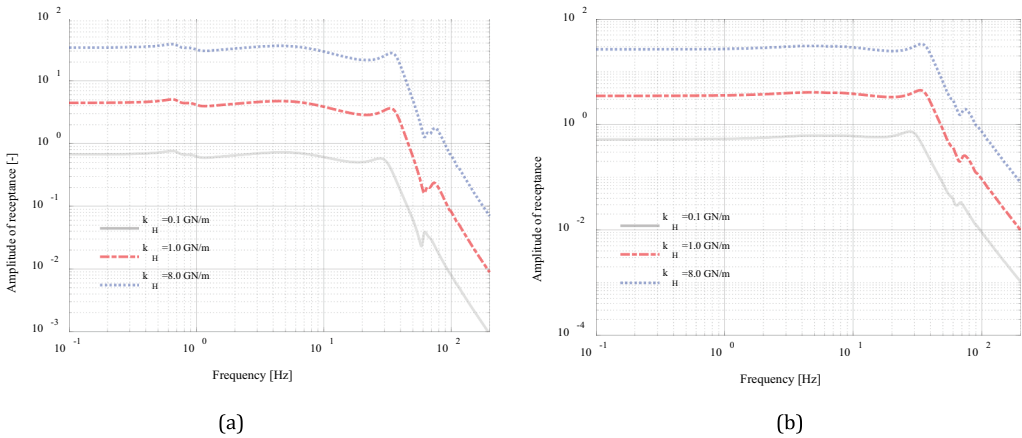


Figure 20. Rear bogie response, normalized with respect to A: (a) Vertical motion, (b) Pitch motion.

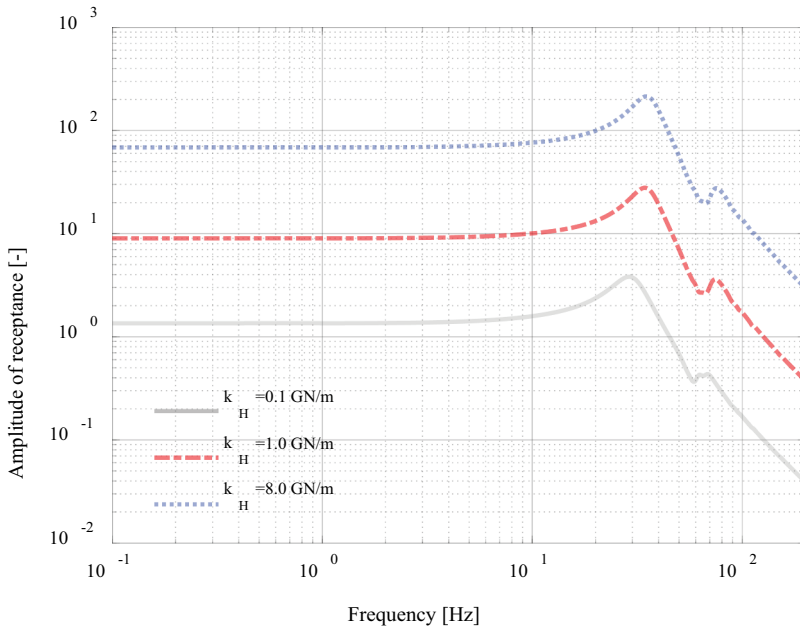


Figure 21. Driving point displacement FRF, wheel vertical motion, normalized with respect to A.

seen that the first peak of the rail receptance increases with increasing contact stiffness first and then converges. The reason for this convergence is that when the contact stiffness is large, the overall supporting stiffness to the wheel is dominated by the track stiffness. Figure 23 shows the dependence of first resonance frequency of the rail on the stiffness of contact spring. From about $k_H = 3.0\text{GN/m}$ the first resonance frequency starts to converge.

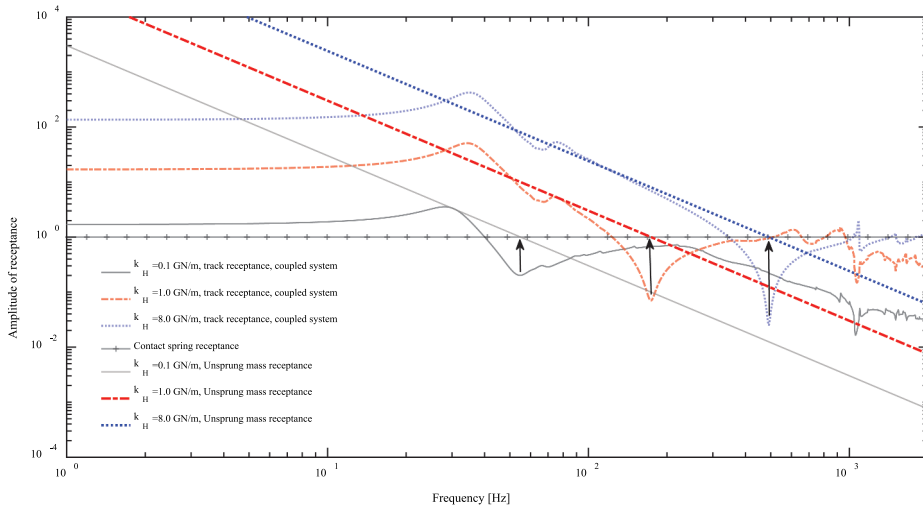


Figure 22. Rail vertical receptance, normalized with respect to A .

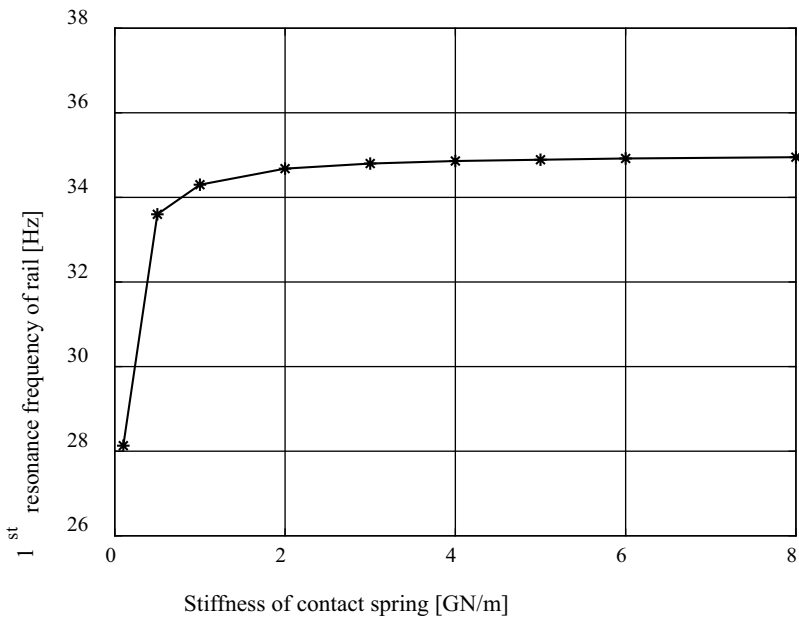


Figure 23. Influence of contact spring stiffness on the 1st resonance frequency f_r of the rail.

5. Conclusions

A fully coupled three-dimensional vehicle-slab track model is employed to investigate the frequency-domain response of the system. Apart from the model validation by time- and frequency-domain response comparisons, the receptances of the vehicle and vertical motion of the rail are thoroughly analysed accounting for the coupling of subsystems

and spatial coherence of multiple wheel-rail contact points caused by multiple wheels. The system responses excited by moving vehicle on irregular track are studied considering the combined effects of the train velocity and the wavelength of vertical track irregularity on the responses are examined in one goal. The critical wavelengths and corresponding critical velocities which cause resonances of different vehicle modes are emphasized. Based on the analysis, the following conclusions can be drawn:

- (1) The resonance frequencies of the vehicle are independent of the track modelling options. However, coupling the track flexibility to the system results in a smaller resonance frequency for the wheel vertical motion. The accuracy of the wheel receptance is important for understanding the wheel/rail interaction and its magnitude.
- (2) Including the track flexibility enables the model to account for effects of multiple wheels and wave reflections in rails between different wheels.
- (3) Although the wave reflections in rails between multiple wheels are important for the overall dynamics of the system, this wave phenomenon does not change the main resonance frequency of the wheels and the rail under the wheels.
- (4) The first resonance frequency of the rail shifts to a lower value when vehicle is considered. At the same time, an antiresonance frequency is introduced at the frequency where the receptance of the contact spring and the receptance of unsprung/wheel mass intersect, namely the antiresonance frequency corresponds to resonance of wheel vertical motion.
- (5) Increasing of the stiffness of the contact spring results in higher resonance frequency of both the wheel and the rail. The first resonance frequency of the rail converges at a certain value of the contact stiffness. The reason is that when the contact stiffness is much larger than the equivalent stiffness from the track, the overall stiffness supporting the wheel converges to the track stiffness and therefore increasing the contact stiffness has marginal influence on the overall stiffness under the wheel. In contrast, higher contact stiffness moves the antiresonance frequency of the rail to higher values and the wheel vibrates on the contact stiffness at this frequency.
- (6) When the excitation frequency $f_{ex} = v/\lambda$ resulting from irregularity coincides with one of the natural frequency of the vehicle, resonances of the vehicle occur. The corresponding critical train velocity and critical wavelength of irregularity are discrete values. The highest critical speeds lead to the largest response of the vehicle since the amplitudes of the harmonic components of irregularities and the associated energy introduced in the system by the track irregularities reduce with decreasing wavelength.

Disclosure statement

The authors declare that they have no conflict of interest.

Funding

This work was supported by the National Natural Science Foundation of China (Grant No.: U1934217).

ORCIDTao Lu  <http://orcid.org/0000-0002-1340-5758>**References**

- [1] Zhai W, Wang K, Cai C. Fundamentals of vehicle–track coupled dynamics. *Veh Syst Dyn.* 2009;47(11):1349–1376.
- [2] Xu L, Zhai W. Train-track coupled dynamics analysis: system spatial variation on geometry, physics and mechanics. *Railway Eng Sci.* 2020;28(1):36–53.
- [3] Zhai W, Xia H, Cai C, et al. High-speed train-track-bridge dynamic interactions-Part I: theoretical model and numerical simulation. *Int J Rail Trans.* 2013;1(1–2):3–24.
- [4] Grassie S, Gregory R, Harrison D, et al. The dynamic response of railway track to high frequency vertical excitation. *J Mech Eng Sci.* 1982;24(2):77–90.
- [5] Knothe K, Wu Y. Receptance behaviour of railway track and subgrade. *Arch Applmech.* 1998;68(7–8):457–470.
- [6] Oregui M, Li Z, Dollevoet R. An investigation into the vertical dynamics of tracks with monoblock sleepers with a 3D finite-element model. *Proc Inst Mech Eng F J Rail Rapid Transit.* 2016;230(3):891–908.
- [7] Cui F, Chew CH. The effectiveness of floating slab track system—Part I. Receptance methods. *Appl Acoust.* 2000;61(4):441–453.
- [8] Hussein MF, Hunt HE. Modelling of floating-slab tracks with continuous slabs under oscillating moving loads. *J Sound Vib.* 2006;297(1–2):37–54.
- [9] Sheng X, Zhong T, Li Y. Vibration and sound radiation of slab high-speed railway tracks subject to a moving harmonic load. *J Sound Vib.* 2017;395:160–186.
- [10] Alabbasi S, Hussein M, Abdeljaber O, et al. A numerical and experimental investigation of a special type of floating-slab tracks. *Eng Struct.* 2020;215:110734.
- [11] Xiao X, Jin X, Wen Z, et al. Effect of tangent track buckle on vehicle derailment. *Multibody Sys Dyn.* 2011;25(1):1–41.
- [12] Sadri M, Steenbergen M. Effects of railway track design on the expected degradation: parametric study on energy dissipation. *J Sound Vib.* 2018;419:281–301.
- [13] Sadri M, Lu T, Zoeteman A, et al. Railway track design & degradation. *MATEC Web of Conferences.* 2018;211:11006.
- [14] Di Gialleonardo E, Braghin F, Bruni S. The influence of track modelling options on the simulation of rail vehicle dynamics. *J Sound Vib.* 2012;331(19):4246–4258.
- [15] Kouroussis G, Connolly DP, Vogiatzis K, et al. Modelling the environmental effects of railway vibrations from different types of rolling stock: a numerical study. *Shock Vib.* 2015;2015:142807.
- [16] Diana G, Cheli F, Collina A, et al. The development of a numerical model for railway vehicles comfort assessment through comparison with experimental measurements. *Veh Syst Dyn.* 2002;38(3):165–183.
- [17] Cheli FE, Corradi RO. On rail vehicle vibrations induced by track unevenness: analysis of the excitation mechanism. *J Sound Vib.* 2011;330(15):3744–3765.
- [18] Lei S, Ge Y, Li Q. Effect and its mechanism of spatial coherence of track irregularity on dynamic responses of railway vehicles. *Mech Syst Signal Process.* 2020;145:106957.
- [19] Wu TX, Thompson DJ. The vibration behavior of railway track at high frequencies under multiple preloads and wheel interactions. *J Acoust Soc Am.* 2000;108(3):1046–1053.
- [20] Wu TX, Thompson DJ. Vibration analysis of railway track with multiple wheels on the rail. *J Sound Vib.* 2001;239(1):69–97.
- [21] Zeng QY, Lou P, Xiang J. The principle of total potential energy with stationary value in elastic system dynamics and its application to the analysis of vibration and dynamic stability. *J Huazhong Univ Sci Technol.* 2002;19(1):7–14.

- [22] Zeng Q, Yang P. The “set-in-right-position” rule for forming structural matrices and the finite truss-element method for space analysis of truss bridges. *J China Railway Soc.* 1986;8(2):48–59.
- [23] Xu L, Lu T. Influence of the finite element type of the sleeper on vehicle-track interaction: a numerical study. *Veh Syst Dyn.* 2020;1–24.
- [24] Chen JB, Peng YB, Li J. A note on the pseudo-excitation method. *Chin J Comput Mech.* 2011;28(2):163–167.
- [25] Johnson K. *Contact mechanics*. UK: Cambridge University Press; 1985. p. 243–283.
- [26] Bian X, Jiang H, Chang C, et al. Track and ground vibrations generated by high-speed train running on ballastless railway with excitation of vertical track irregularities. *Soil Dyn Earthq Eng.* 2015 Sep 1;76:29–43. .
- [27] Hung CF, Hsu WL. Influence of long-wavelength track irregularities on the motion of a high-speed train. *Veh Syst Dyn.* 2018;56(1):95–112.

Appendix

Table A1. Main parameters of the vehicle.

Notation	Parameter (unit)	Values
M_c	Car body mass (kg)	49080
M_t	Bogie mass (kg)	4420
M_w	Wheelset mass (kg)	1680
I_{cx}	Mass moment of inertia of car body about X-axis (kg m ²)	65700
I_{cy}	Mass moment of inertia of car body about Y-axis (kg m ²)	1698400
I_{cz}	Mass moment of inertia of car body about Z-axis (kg m ²)	1447100
I_{tx}	Mass moment of inertia of bogie about X-axis (kg m ²)	1576
I_{ty}	Mass moment of inertia of bogie about Y-axis (kg m ²)	4902
I_{tz}	Mass moment of inertia of bogie about Z-axis (kg m ²)	3551
I_{wx}	Mass moment of inertia of wheelset about X-axis (kg m ²)	773.3
I_{wy}	Mass moment of inertia of wheelset about Y-axis (kg m ²)	130
I_{wz}	Mass moment of inertia of wheelset about Z-axis (kg m ²)	770
k_{px}	Stiffness coefficient of primary suspension along X-axis (MN/m)	1.24
k_{py}	Stiffness coefficient of primary suspension along Y-axis (MN/m)	1.24
k_{pz}	Stiffness coefficient of primary suspension along Z-axis (MN/m)	1.27
k_{sx}	Stiffness coefficient of secondary suspension along X-axis (MN/m)	0.11
k_{sy}	Stiffness coefficient of secondary suspension along Y-axis (MN/m)	0.11
k_{sz}	Stiffness coefficient of secondary suspension along Z-axis (MN/m)	0.27
c_{pz}	Damping coefficient of primary suspension along Z-axis (kN s/m)	65
c_{sy}	Damping coefficient of secondary suspension along Y-axis (kN s/m)	5.4
c_{sz}	Damping coefficient of secondary suspension along Z-axis (kN s/m)	16.5
L_c	Semi-longitudinal distance between bogies (m)	7.85
L_t	Semi-longitudinal distance between wheelsets in bogie (m)	1.25
R_0	Wheel radius (m)	0.43

Table A2. Main parameters of the track structures.

Notation	Parameter (unit)	Values
E_r	Elastic modulus of the rail (N/m ²)	2.059×10^{11}
ρ_r	Mass of the rail per unit length (kg/m)	60.64
I_{ry}	Rail second moment of the area about the Y axis (m ⁴)	3.215×10^{-5}
I_{rz}	Rail second moment of the area about the Z axis (m ⁴)	5.24×10^{-6}
G_k	Rail torsional stiffness (N m/rad)	1.9587×10^5
k_{tz}	Fastener stiffness in the vertical direction (N/m)	3×10^7
k_{ry}	Fastener stiffness in the lateral direction (N/m)	3.5×10^7
c_{tz}	Fastener damping in the vertical direction (N s/m)	2.5×10^4
c_{ry}	Fastener damping in the lateral direction (N s/m)	2.5×10^4
E_t	Elastic modulus of the slab (N/m ²)	3.6×10^{10}
μ_t	Poisson ratio of the slab	0.25
m_t	Mass per unit volume of the slab (kg/m ³)	2500
H_t	Height of the slab (m)	0.19
L_t	Length of the slab (m)	4.95
W_t	Width of the slab (m)	2.40
k_{tz}	Equivalent vertical stiffness coefficient of the CA layer (N/m)	1.3×10^9
c_{tz}	Equivalent vertical damping coefficient of the CA layer (N/m)	1.0×10^4
k_{ty}	Equivalent vertical stiffness coefficient of the CA layer (N/m ²)	6×10^7
c_{ty}	Equivalent vertical damping coefficient of the CA layer (N/m)	1.0×10^4